Auxiliary Material Submission for manuscript

"How much did Glacial North Atlantic Water shoal?"

Geoffrey Gebbie

Physical Oceanography Department, Woods Hole Oceanographic Institution

Contents

1. Detailed inverse problem formulation

The method is detailed through a set of constraints on the problem unknowns: the water-mass proportions, $\mathbf{m}$, all relevant tracer distributions on an underlying grid, $\mathbf{c}_k$, and any remineralization source for nonconservative tracers, $\mathbf{q}$.

Tracer observations are imposed without loss of generality as an equation: $\sum_{k=1}^{K}\{\mathcal{E}_k[\mathbf{c}_k]\} = \mathbf{y} + \mathbf{n}$, where there are K modeled tracers, $\mathcal{E}_k$ is a potentially nonlinear mapping of the gridded fields onto the observational location of observational type and performs the "proxy" step of relating the modeled tracers to observed quantities, $\mathbf{y}$ is the list of many disparate observations, and $\mathbf{n}$ is the noise in the observations. This form takes into account the fact that paleo-observations may depend upon multiple seawater tracers (e.g., $\delta^{18}O_c$ requires temperature and seawater $\delta^{18}O$), and that this relationship may be nonlinear (e.g., $\delta^{18}O_c$ requires in-situ rather than potential temperature, and Cd_w is nonlinearly related to phosphate). If the tracer observations are restricted to those that are explicitly modeled (e.g., $\delta^{18}O_w$) or to climatologies where a tracer value is available at all gridded locations (e.g., WOCE salinity and nutrients), the nonlinear function $\mathcal{E}_k$ is reduced to a matrix.

The tracers are constrained by non-observational information, as well. These constraints include gravitational stability, non-negativity constraints expressed in terms of barrier functions, and $\delta^{13}C_{as}$ being within the range that has been found in modern-day observations and models ($\pm 1‰$). To keep the solution within reasonable bounds and also improve the efficiency of the solution method, the surface tracer deviation is defined relative to a first guess, $\Gamma\mathbf{c}_{bk} = \mathbf{c}_{0k} + \mathbf{n}_{bk}$, where Γ picks out the surface values from the global distribution, $\mathbf{c}_{bk}$ is the surface concentration, $\mathbf{c}_{0k}$ is the first guess, and $\mathbf{n}_{bk}$ is surface deviation away from the first guess for tracer k. Equations for gravitational stability, non-negativity, and the range of $\delta^{13}C_{as}$ are symbolically lumped into one set of nonlinear equations for the derivation here:

$\mathcal{F}_c[\mathbf{c}_k] = \mathbf{n}_c$, where $\mathbf{n}_c$ is the degree to which these equations are inexact.

No direct observations of the interior tracer sources, $\mathbf{q}$, or the water-mass pathway vector, $\mathbf{m}$, are available, so these unknowns are simply kept within a reasonable range of a first-guess where, for example, $\mathcal{F}_q[\mathbf{q}, \mathbf{q}_0] = \log(\mathbf{q}) - \log(\mathbf{q}_0) = \mathbf{n}_q$, is the deviation from the first guess local sources, $\mathbf{q}_0$. The difference of logarithms assumes and enforces the source to be positive, and for the order of magnitude of the deviation to be penalized. The pathway parameters, $\mathbf{m}$, are penalized using an similar nonlinear function, $\mathcal{F}_m$.

1.1. Steady state constraint

Equation (1) in the main text is put into the form of a steady-state constraint by putting all terms on the left hand side: $f_{ik} = \sum_{j=1}^{N} m_{ij}\, c_{jk} + r_k q_i - c_{ik} = 0$, for all interior locations i and tracers k, with $f_{ik} = c_{ik} - c_{bk}$ at the surface. Mass conservation is one of these constraints, here denoted to be the $k = K+1$ tracer: $f_{i,K+1} = \sum_{j=1}^{N} m_{ij} - 1$, found by substituting $c_{j,K+1} = 1$, $c_{i,K+1} = 1$, and $r_{K+1} = 0$ above. Any steady-state tracer, k, must satisfy $\mathcal{F}_k = 0$ which is defined by appending f_{ik} at all i locations.

1.2. Solution technique

All constraints are enforced through the method of Lagrange multipliers. For equations that contain noise, a weighted quadratic form, $\mathbf{n}^T \mathbf{W} \mathbf{n}$, is added to the Lagrangian function in order to minimize the sum of squared noise elements. For the steady-state constraint that does not contain noise, a Lagrange multiplier term is appended to the function for strict enforcement. Solving for $\mathbf{n}$ in terms of the other unknowns of the problem, the Lagrangian function is

$$
\begin{aligned}
\mathcal{L}[\mathbf{c}_k, \mathbf{q}, \mathbf{m}] \;=\; & \left(\sum_{k=1}^{K}\{\mathcal{E}_k[\mathbf{c}_k]\} - \mathbf{y}\right)^T \mathbf{W}\left(\sum_{k=1}^{K}\{\mathcal{E}_k[\mathbf{c}_k]\} - \mathbf{y}\right) & (1) \\
+\; & \sum_{k=1}^{K}\{(\Gamma\mathbf{c}_k - \mathbf{c}_{0k})^T \mathbf{S}_k(\Gamma\mathbf{c}_k - \mathbf{c}_{0k})\} & (2) \\
+\; & \mathcal{F}_c[\mathbf{c}_k]^T \mathbf{W}_c \mathcal{F}_c[\mathbf{c}_k] + \mathcal{F}_q[\mathbf{q}]^T \mathbf{S}_q \mathcal{F}_q[\mathbf{q}] + \mathcal{F}_m[\mathbf{m}]^T \mathbf{S}_m \mathcal{F}_m[\mathbf{m}] & (3) \\
+\; & \sum_{k=1}^{K+1} \mu_k^T\, \mathcal{F}_k[\mathbf{c}_k, \mathbf{q}, \mathbf{m}], & (4)
\end{aligned}
$$

where $\mathbf{W}$ is the observational weighting matrix and $\mathbf{W}_c$ is the weighting of the additional tracer constraints. $\mathbf{S}_k$, $\mathbf{S}_q$ and $\mathbf{S}_m$ are scaling matrices that enforce bounds and smoothness on the expected deviation in each surface tracer, interior source, and pathways, respectively. There is one Lagrange multiplier vector, μ_k, for each of the $K+1$ steady-state equations, and note that the Lagrange multiplier terms do not alter the numerical value of the function.

For tracer climatologies, $\mathbf{W}$ is diagonal with the inverse of published error estimates squared. For the sediment core data, the $\mathbf{W}$ matrix has the same form, and the additional constraint that there be no systematic misfit with depth is appended. Finding the model-data bias as a function of depth is a linear operation, $\mathbf{Zn}$, an additional constraint can be added to the previous cost function term. The weighting matrix then becomes $\mathbf{W} + \mathbf{Z}^T \mathbf{W}_z \mathbf{Z}$, a nondiagonal matrix. $\mathbf{W}_z$ is chosen based on the expected vertical systematic error that arises from random noise.

The minimum of $\mathcal{L}$ is found by seeking a stationary point of the terms (1)-(4). The partial derivative with respect to each tracer gives a set of (adjoint) equations that is solved for the Lagrange multipliers by an LU decomposition. The Lagrange multiplier vectors yield information about how the Lagrangian function will change given a change in a subset the unknowns, $\mathbf{c}_{bk}$, $\mathbf{q}$, and $\mathbf{m}$, where these variables contain all information necessary to solve for the global tracer distributions. A quasi-Newton gradient descent method uses this information to iteratively search for the minimum $\mathcal{L}$ [*Nocedal*, 1980; *Gilbert and Lemaréchal*, 1989]. All controls (independent unknowns) are preconditioned by the Cholesky decomposition of the respective scaling matrix, $\mathbf{S}$, to improve performance.

2. Model-Data Misfits

The use of nondiagonal matrices, as described in the method above, puts emphasis on capturing the vertical structure of the observations. The model-data misfit as a function of depth is included in Auxiliary Figures 1-2. Additionally, we include a meridional section of the $\delta^{13}C$ and $\delta^{13}C_{as}$ distributions with pointwise misfits denoted (Auxiliary Figures 3-4). These

figures indicate that the vertical structure of the observations is captured within the expected errors.

3. Water-mass analysis

A phosphate-δ^{13}C diagram puts the geographic Atlantic section into the context of water-mass endmember values and mixing lines. At the core sites that contain measurements of both Cd and δ^{13}C, we translate Cd to phosphate following *Elderfield and Rickaby* [2000] and plot δ^{13}C-PO$_4$ property combinations, where δ^{13}C$_{as}$ isolines are straight in this property-property space (Auxiliary Figure 5). Even though the δ^{13}C$_{as}$ map of this work appears to have a different vertical structure from the map of *Marchitto and Broecker* [2006], the dominant linear relationship between δ^{13}C and phosphate is captured at the core sites, including the modern-day slope of -0.6‰/μmol/kg steepening to -1.3‰/μmol/kg during the LGM. All modern-day δ^{13}C$_{as}$ core values and all but three LGM δ^{13}C$_{as}$ core values are within 0.5‰ of zero after accounting for observational noise, an indication that air-sea disequilbrium signatures are small in the deep ocean if the recent burning of fossil fuels is eliminated [e.g., *Olsen and Ninnemann*, 2010] and that the water-mass signal in δ^{13}C$_{as}$ is smaller than the signal of biological effects.

The change in phosphate-δ^{13}C slope is due to the "effective endmembers," defined to be the most representative properties in a given surface region [*Gebbie and Huybers*, 2011]. Here we define seven surface regions in the Atlantic sector (see Figure 5 for definitions), where the endmembers are computed by weighting the surface tracer concentrations by the Atlantic interior volume filled by each location. The modern-LGM difference in slope is due to the change in δ^{13}C$_{as}$ of the primary water-masses that make the general linear trend. In the modern-day, the Labrador and GIN Seas have relatively-high δ^{13}C but low δ^{13}C$_{as}$ (-0.4‰). Weddell Sea Water has low δ^{13}C but high δ^{13}C$_{as}$ (0.3‰), with the net effect being a flattening of the overall slope. In the LGM, the pattern is reversed, with relatively-low δ^{13}C and δ^{13}C$_{as}$ being colocated in the Southern Ocean, and both quantities relatively high in the

North Atlantic. The net result is a steepened slope in the LGM.

Even though the effective endmember values aren't strongly constrained by observations, there is general agreement between our study and previous studies. Glacial endmember estimates were previously estimated by extrapolation of mixing lines in a property-property diagram [AABW: 0.6 to 0.8 nmol/kg, -0.5 to -1.0‰ δ^{13}C, *Marchitto and Broecker*, 2006]. Here, we refine their estimates (0.85 nmol/kg, -0.9‰), but recognize that any additional Southern Ocean observations could alter them. Glacial Antarctic Intermediate Water δ^{13}C is reconstructed to be 0.2-0.3‰, in accord with *Curry and Oppo* [2005]. We also find a large gradient between upper and lower North Atlantic Water properties, consistent with increased sea ice and unutilized nutrients in the Nordic Seas [*Mix and Fairbanks*, 1985], that further complicates the finding of an interface between northern and southern source waters, as lower North Atlantic Water is more similar to Antarctic water. Other endmember values will need to be refuted or refined with additional observations. For example, the Atlantic-wide range of Cd is 50% greater during the LGM, which together with the conservation of global phosphate inventory, requires North Atlantic source waters to be even more depleted than they are today (<0.1 nmol/kg).

Figure 6.

Figure 7.

Figure 8.

Figure 9.

Figure 10.

Figure 11.

Figure 12.

References

Curry, W., and D. Oppo (2005), Glacial water mass geometry and the distribution of δ^{13}C of $\sum$CO$_2$ in the Western Atlantic Ocean, *Paleoceanography*, *20*, 10.1029/2004PA001,021.

Elderfield, H., and R. Rickaby (2000), Oceanic Cd/P ratio and nutrient utilization in the glacial Southern Ocean, *Nature*, *405*(6784), 305–310.

Gebbie, G., and P. Huybers (2011), How is the ocean filled?, *Geophys. Res. Lett.*, *38, L06604, doi:10.1029/2011GL046769*.

Gilbert, J. C., and C. Lemaréchal (1989), Some numerical experiments with variable-storage quasi-Newton algorithms, *Math. Program.*, *45*, 407–435.

Marchitto, T., and W. Broecker (2006), Deep water mass geometry in the glacial Atlantic Ocean: A review of constraints from the paleonutrient proxy Cd/Ca, *Geochemistry Geophysics Geosystems*, *7*(12), Q12,003.

Mix, A. C., and R. G. Fairbanks (1985), North Atlantic surface-ocean control of Pleistocene deep-ocean circulation, *Earth and Planetary Science Letters*, *73*(2), 231–243.

Nocedal, J. (1980), Updating quasi-Newton matrices with limited storage, *Mathematics of computation*, *35*(151), 773–782.

Olsen, A., and U. Ninnemann (2010), Large δ13C gradients in the preindustrial north atlantic revealed, *Science*, *330*(6004), 658.

Figure Captions
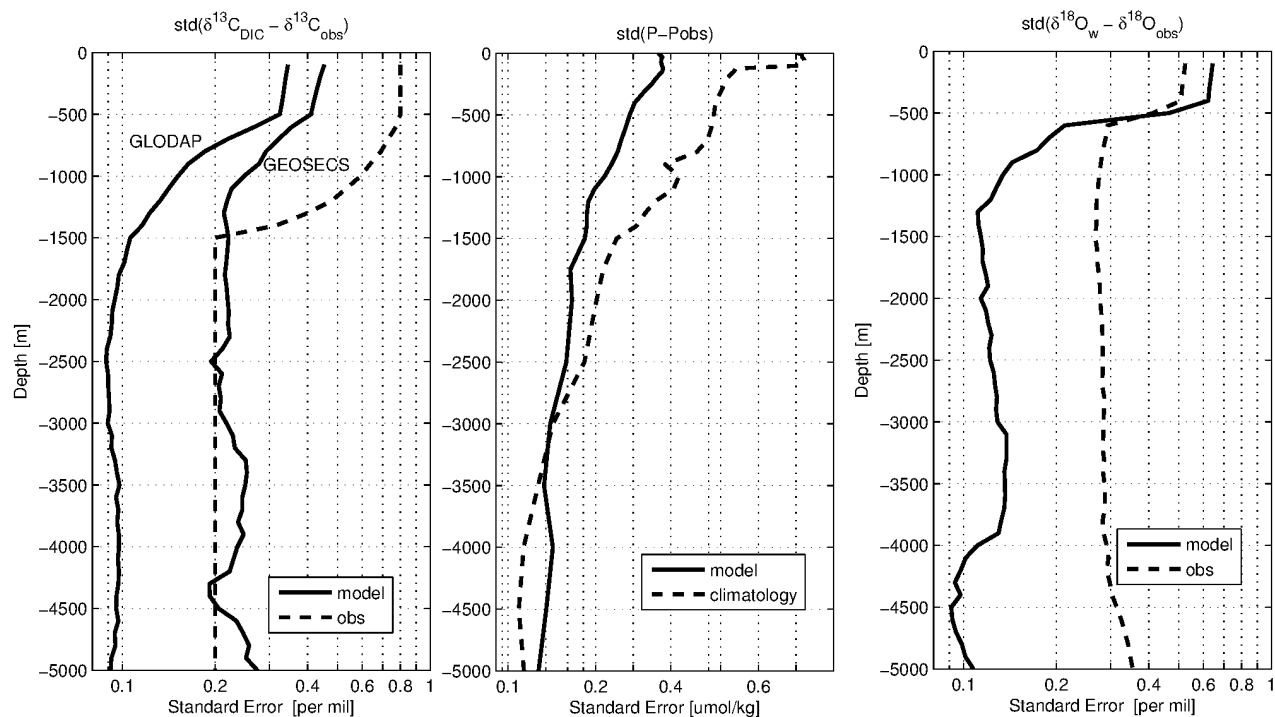
Figure 1. Comparison of reconstructed error relative to expected error as a function of depth: standard deviation of model-observation misfit (*solid lines*) over a 1000 meter running interval for $\delta^{13}C_{DIC}$ (*left panel*), PO_4 (*middle panel*), and $\delta^{18}O_w$ (*right panel*), and the expected standard error from published sources or subjective choice as used in the reconstruction method (*dashed lines*).
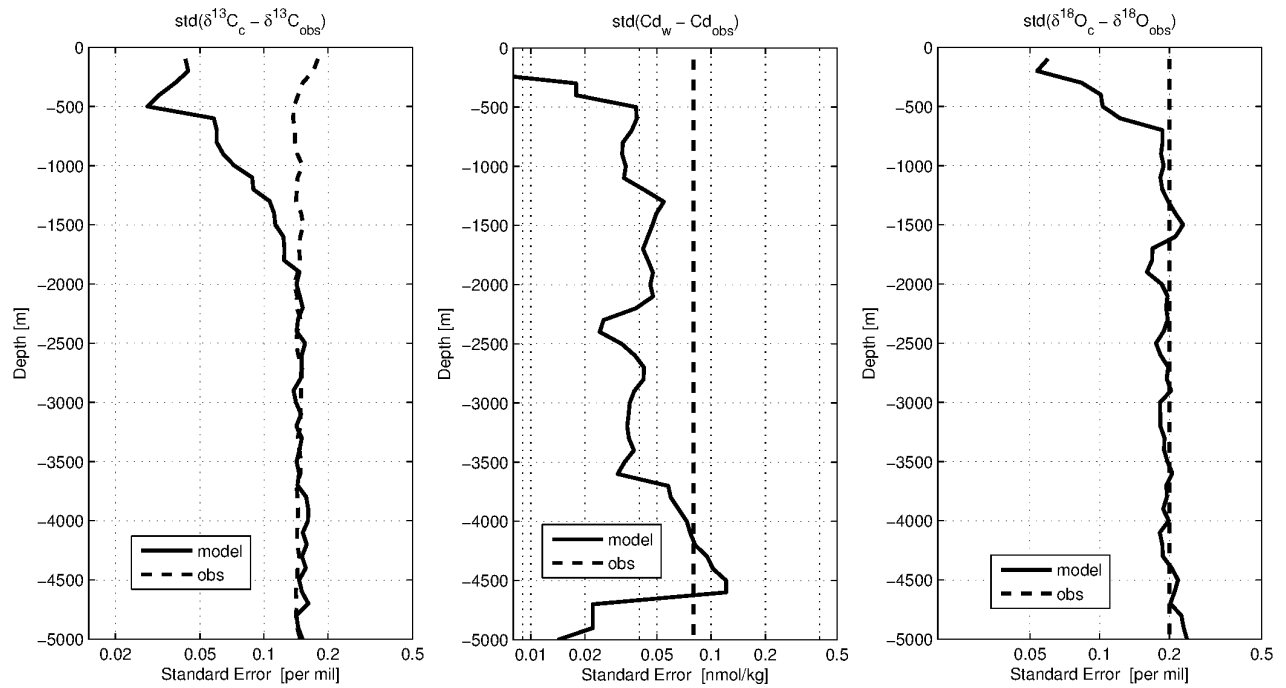
Figure 2. Error statistics of the LGM solution for δ^{13}C (*left panel*), Cd (*middle panel*), and δ^{18}O (*right panel*) data from benthic foraminiferal calcite. The reconstructed standard error over 1000 meter running depth intervals (σ, *bold solid line*) is compared to the expected standard error (*bold dashed line*). The absolute value of the mean misfit or offset (μ) is compared between the reconstruction (*thin solid line*) and the expected 95% confidence interval (*thin dashed line*).
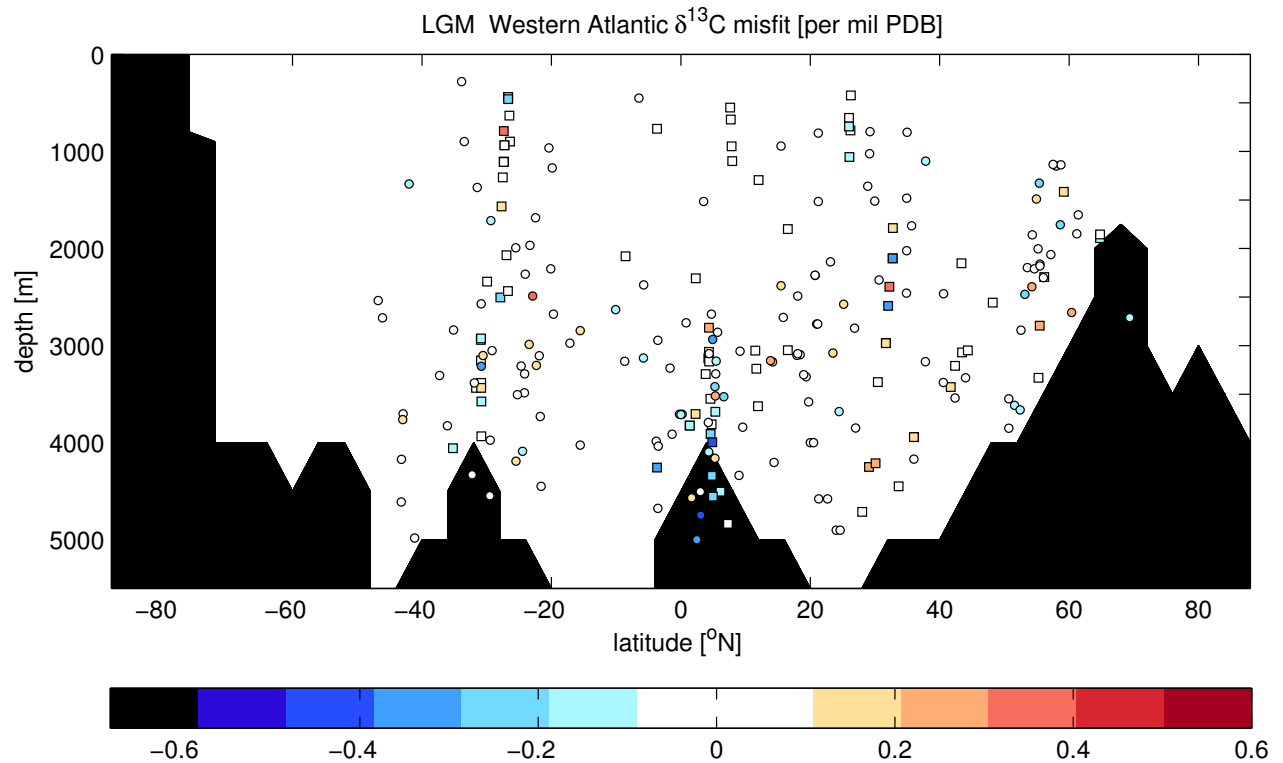
Figure 3. The glacial meridional sections collapse all data points onto a western or eastern section. To account for zonal variations in the core locations, we plot the model-data misfit at the actual locations of the data. The model-data misfit is included for LGM $\delta^{13}C_c$. Squares represent data locations in the western Atlantic (west of $35°$W) and circles represent the eastern Atlantic.
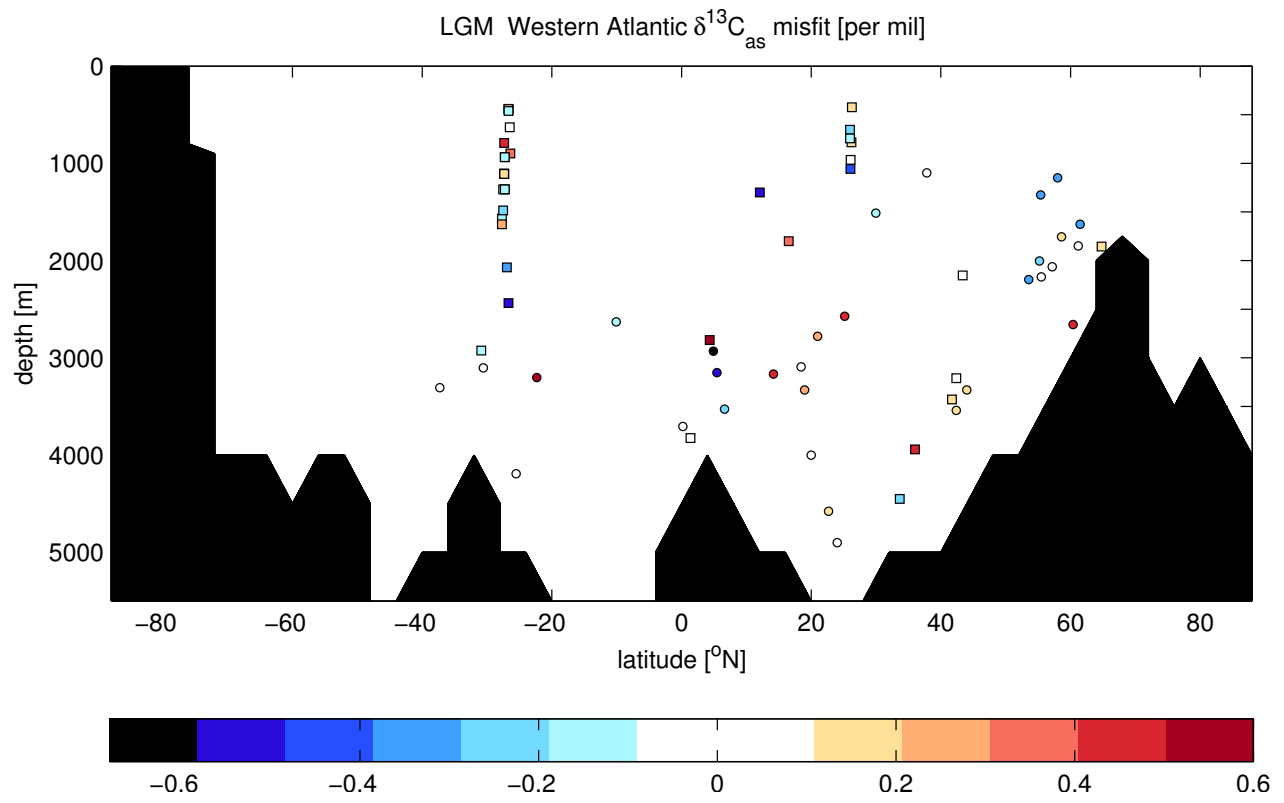
Figure 4. Same as the previous figure but for $\delta^{13}C_{as}$ inferred from core locations with both $\delta^{13}C_c$ and Cd measurements.
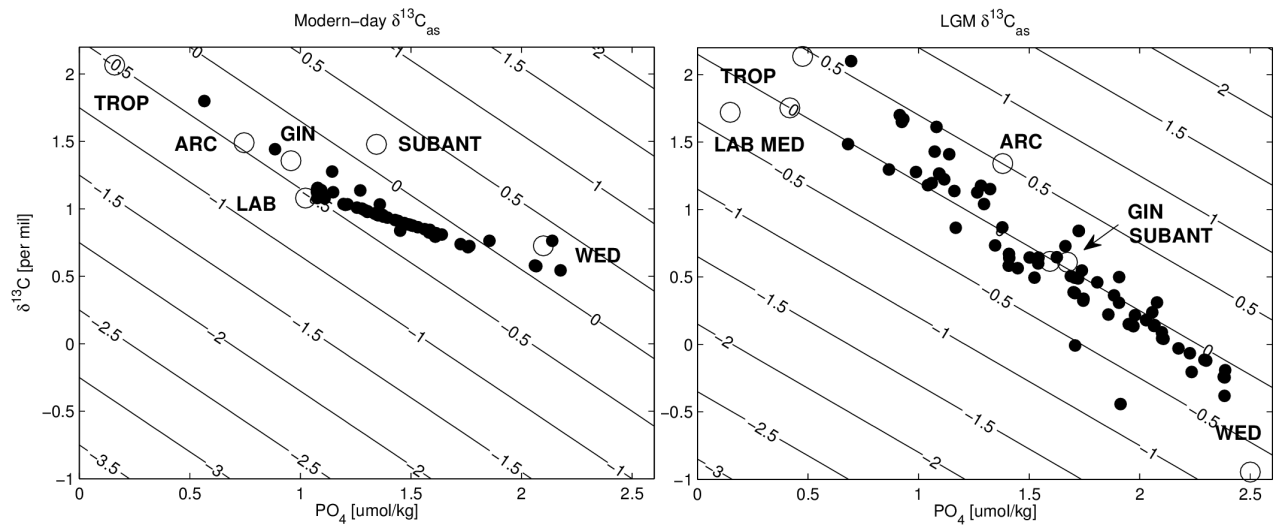
Figure 5. Water mass diagrams in phosphate-δ^{13}C space for the modern (*left panel*) and LGM (*right panel*). Reconstructed tracer-tracer values at the locations with Cd and δ^{13}C observations (*black circles*) are placed into the context of $\delta^{13}C_{as}$ (*background contours*). The effective end-member values (*open circles*) enclose the data points, and are defined for the following surface regions: Weddell Sea (WED), Atlantic Subantarctic (SUBANT), Labrador and Irminger Seas (LAB), Greenland-Icelandic-Norwegian Seas (GIN), Arctic (ARC), Mediterranean (MED), and subtropics/tropics (TROP). The modern-day MED endmember is offscale (0.2μmol/kg, 2.2‰).
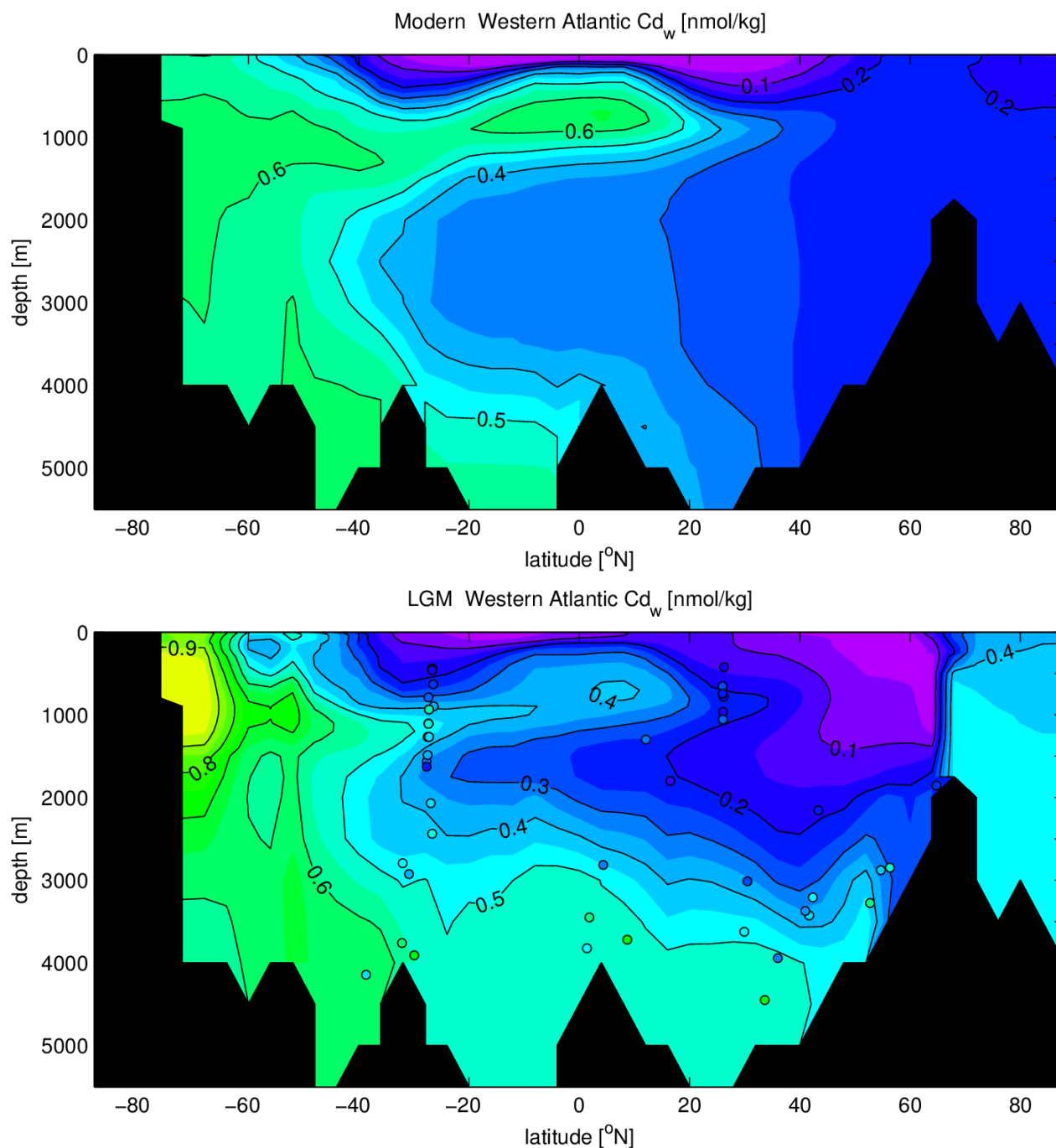
Figure 6. Western Atlantic Property Atlas: Additional meridional sections that compare modern and LGM properties along the western Atlantic GEOSECS track are included here for the following properties: Cd_w (this figure) and $\delta^{18}O_c$ (next figure). Similar figures for $\delta^{13}C$, $\delta^{13}C_{as}$, preformed $\delta^{13}C$, and North Atlantic Water concentration, $\mathbf{g}_{north}$, are included in the main text.
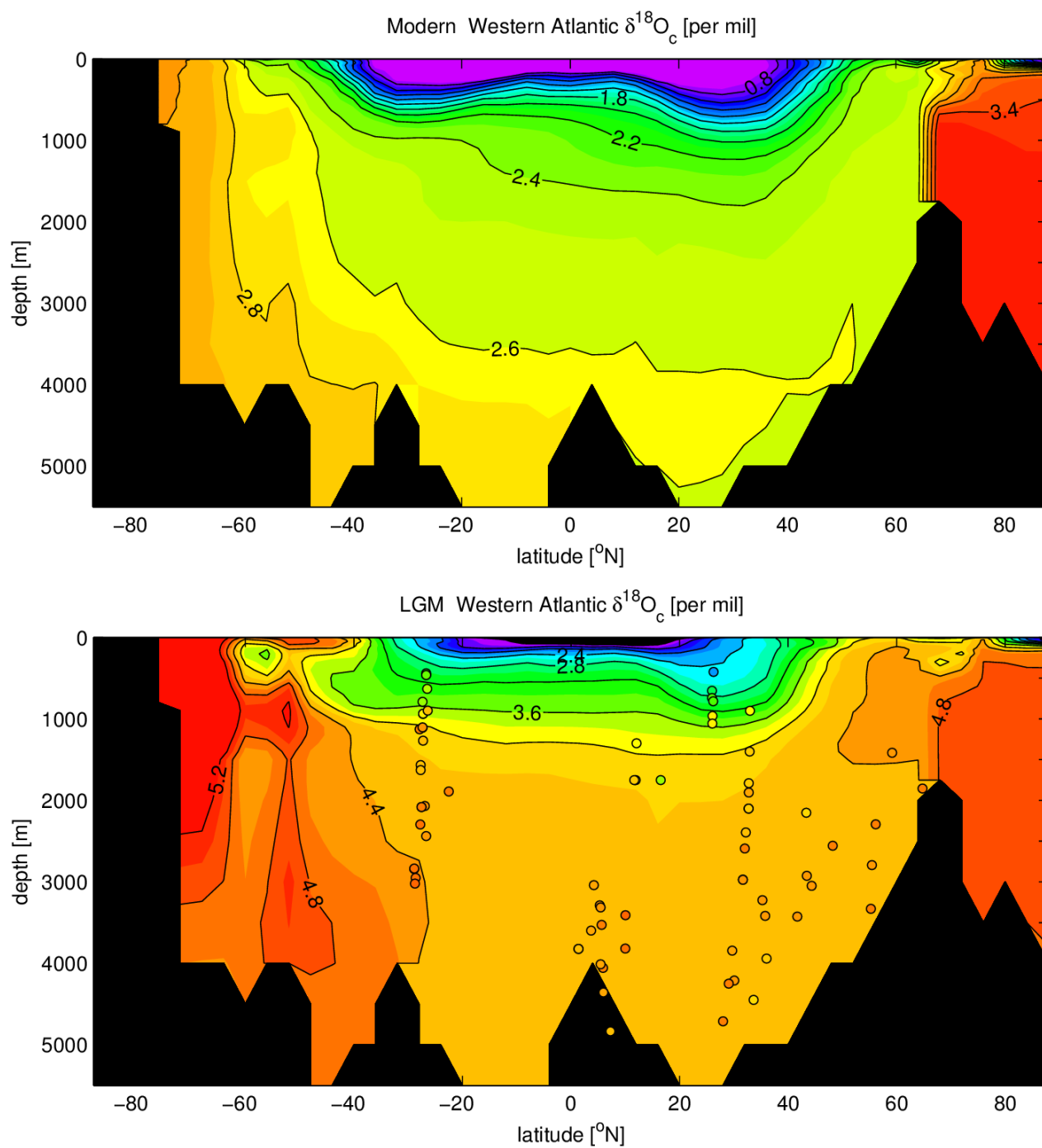
14

Figure 7. Same as previous figure but for $\delta^{18}O_c$.

Modern Eastern Atlantic δ^{13}C [per mil PDB]

LGM Eastern Atlantic δ^{13}C [per mil PDB]
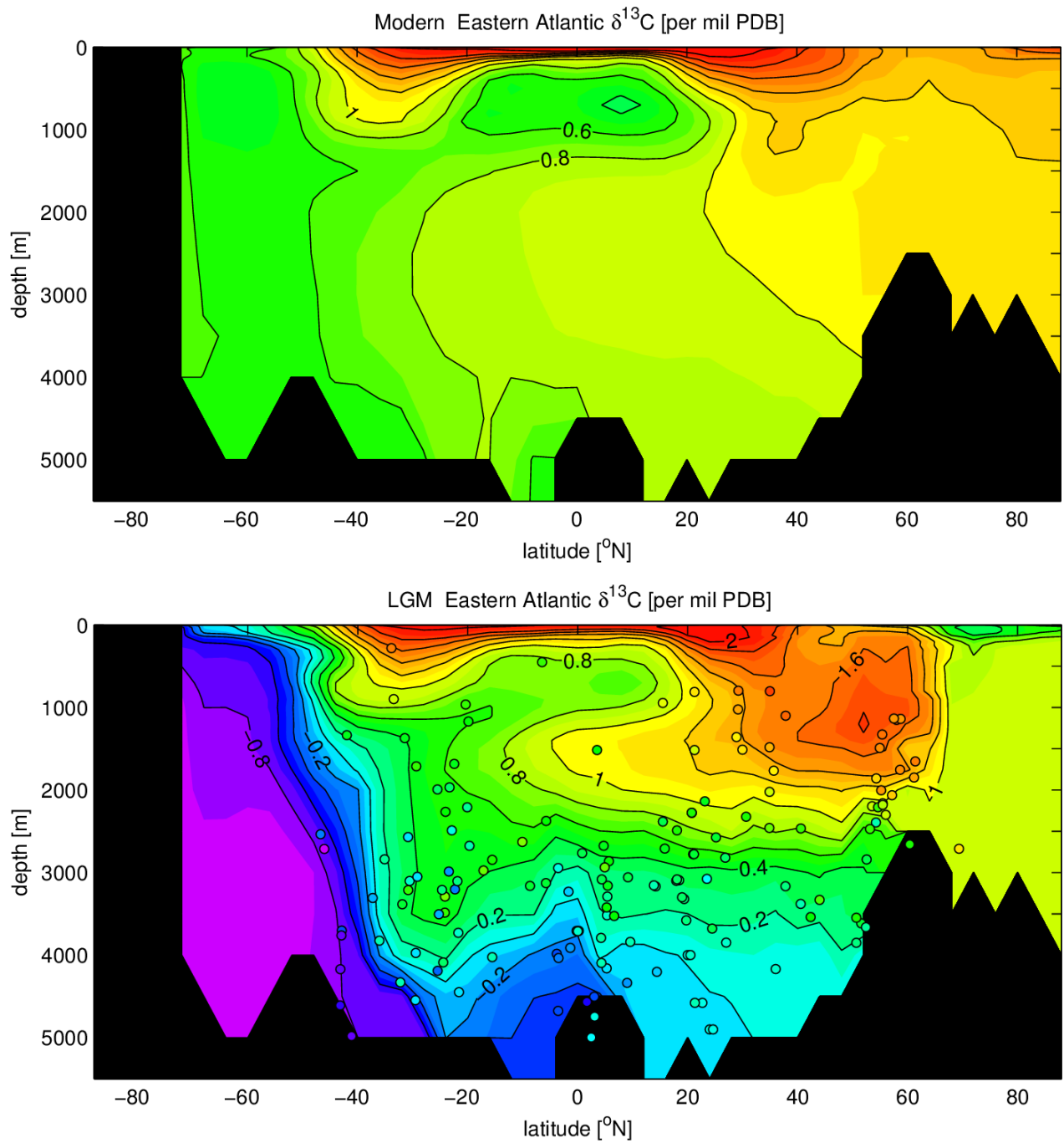
Figure 8. Eastern Atlantic Property Atlas: Meridional sections along the A16 WOCE transect are included here for the following properties: δ^{13}C, δ^{13}C$_{as}$, Cd$_w$, δ^{18}O$_c$, and North Atlantic Water concentration, $\mathbf{g}_{north}$.
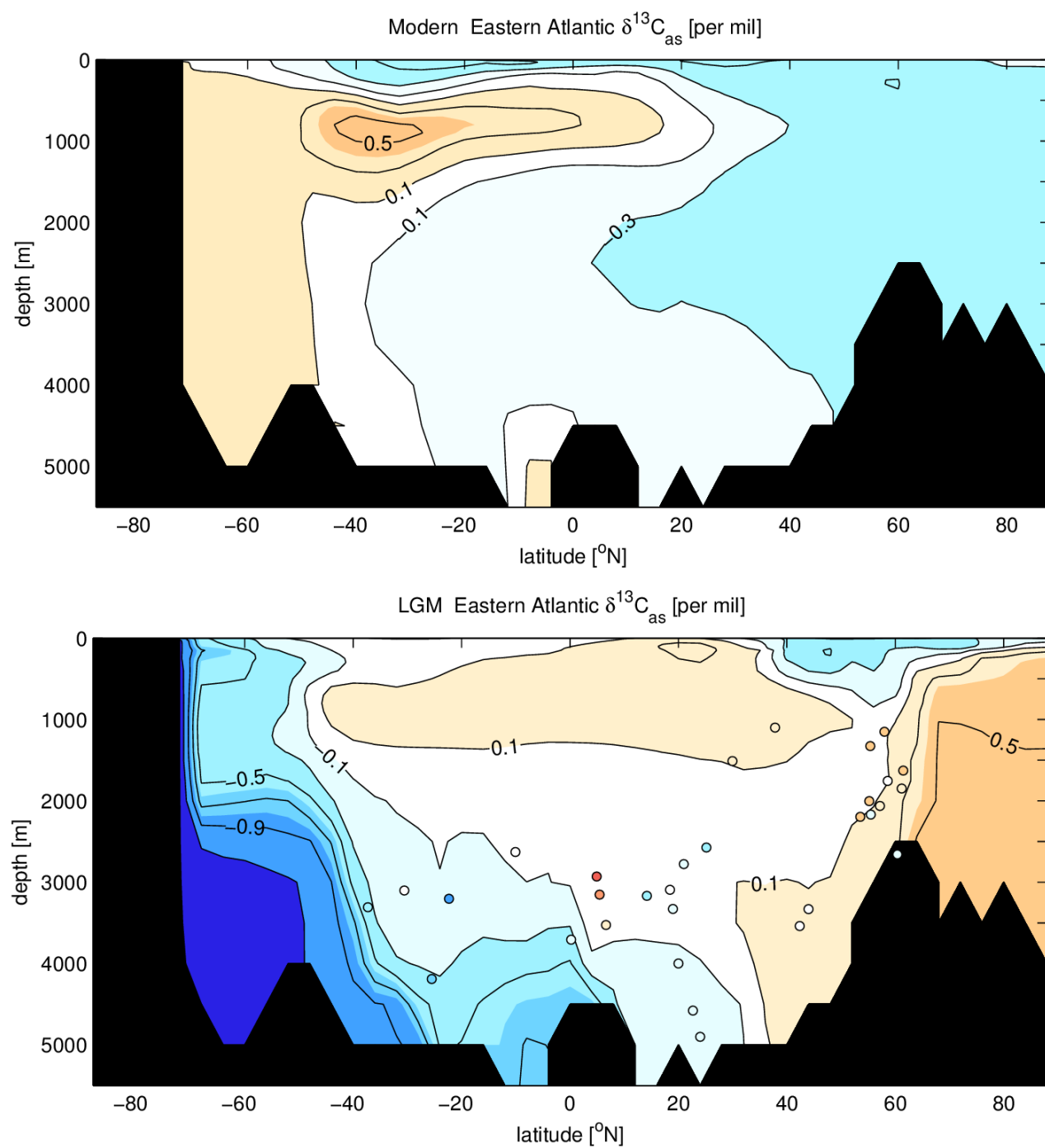
Figure 9. Same as Figure 8, but for $\delta^{13}C_{as}$.
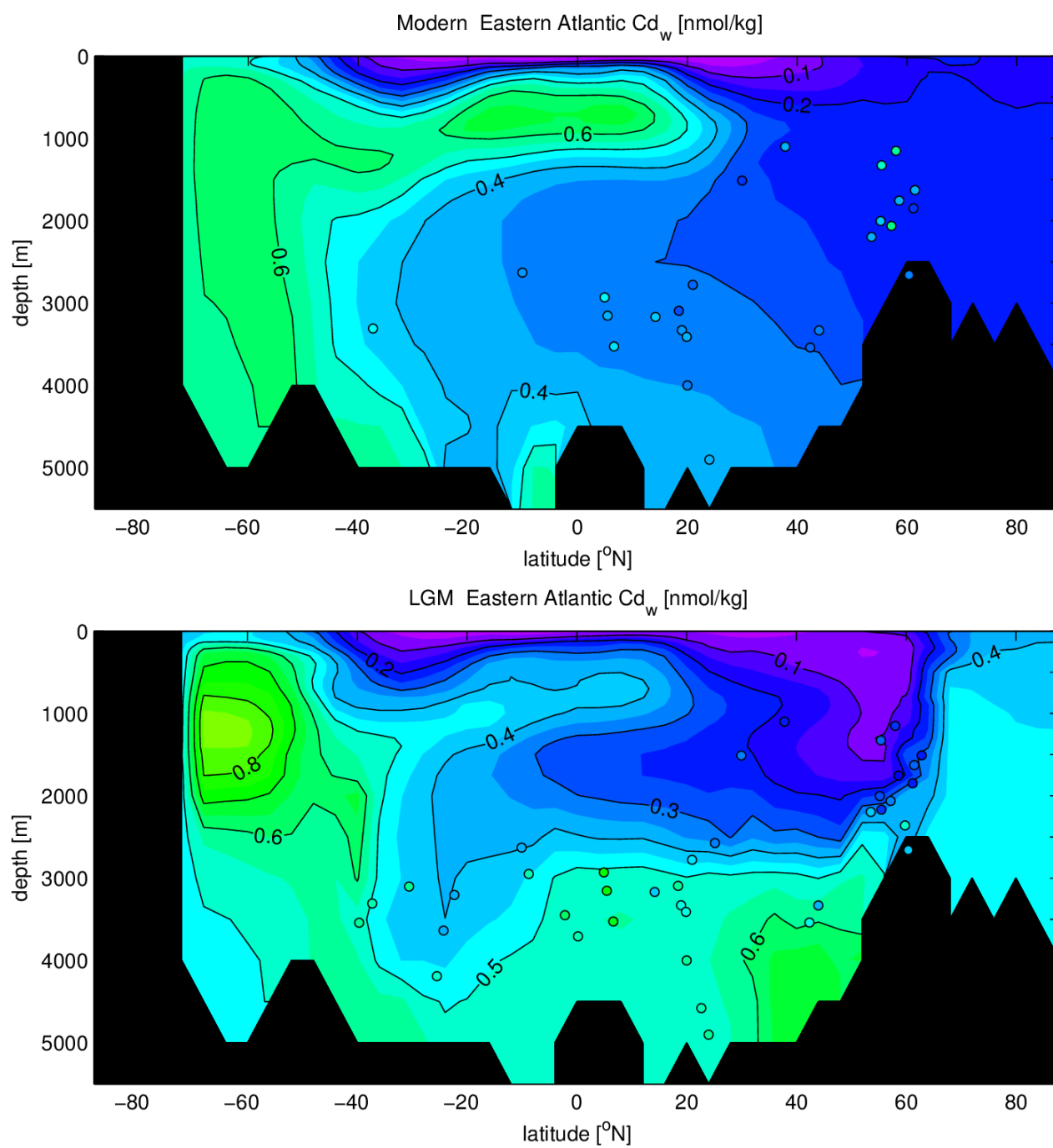
Figure 10. Same as Figure 8, but for seawater Cd.

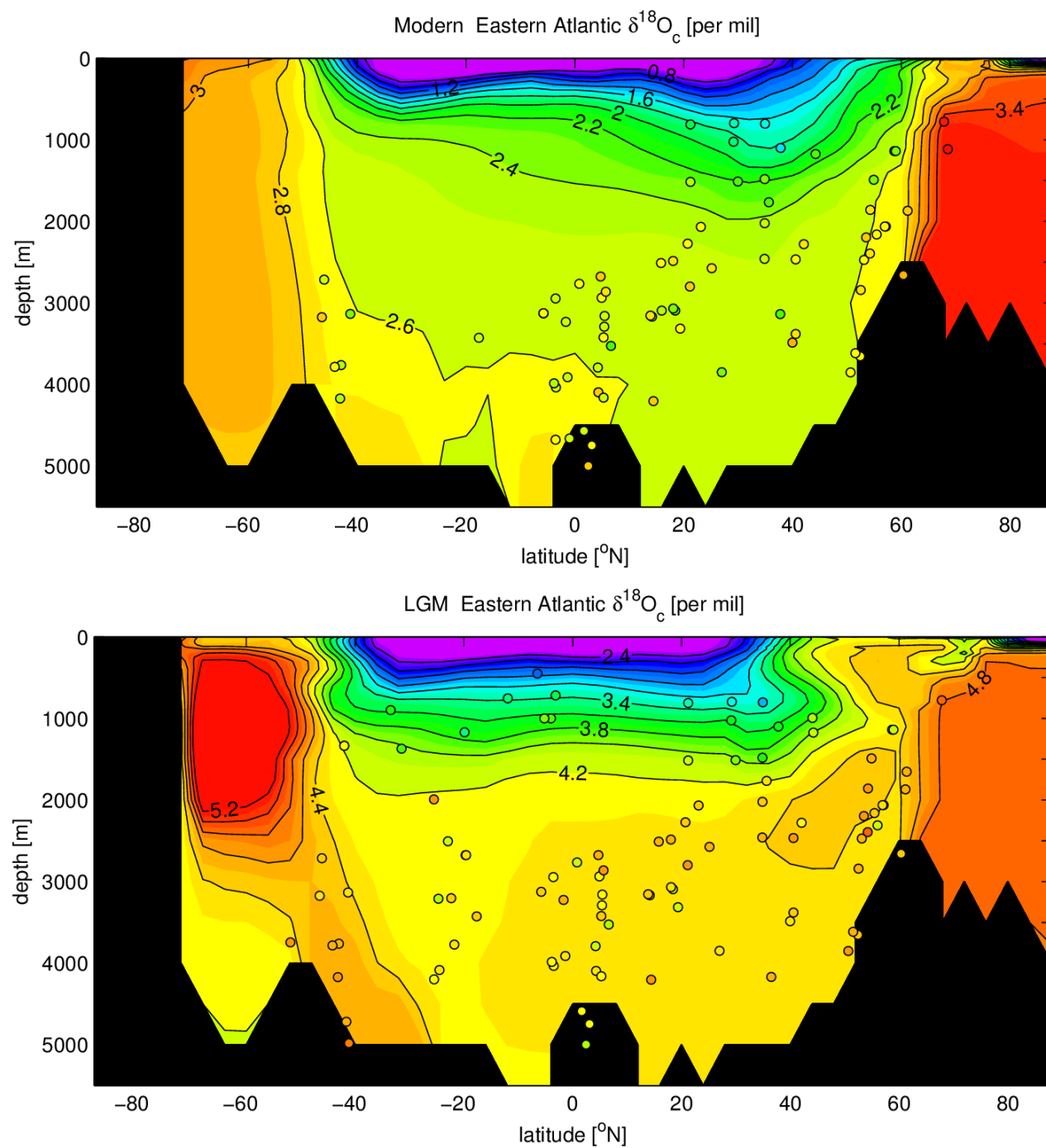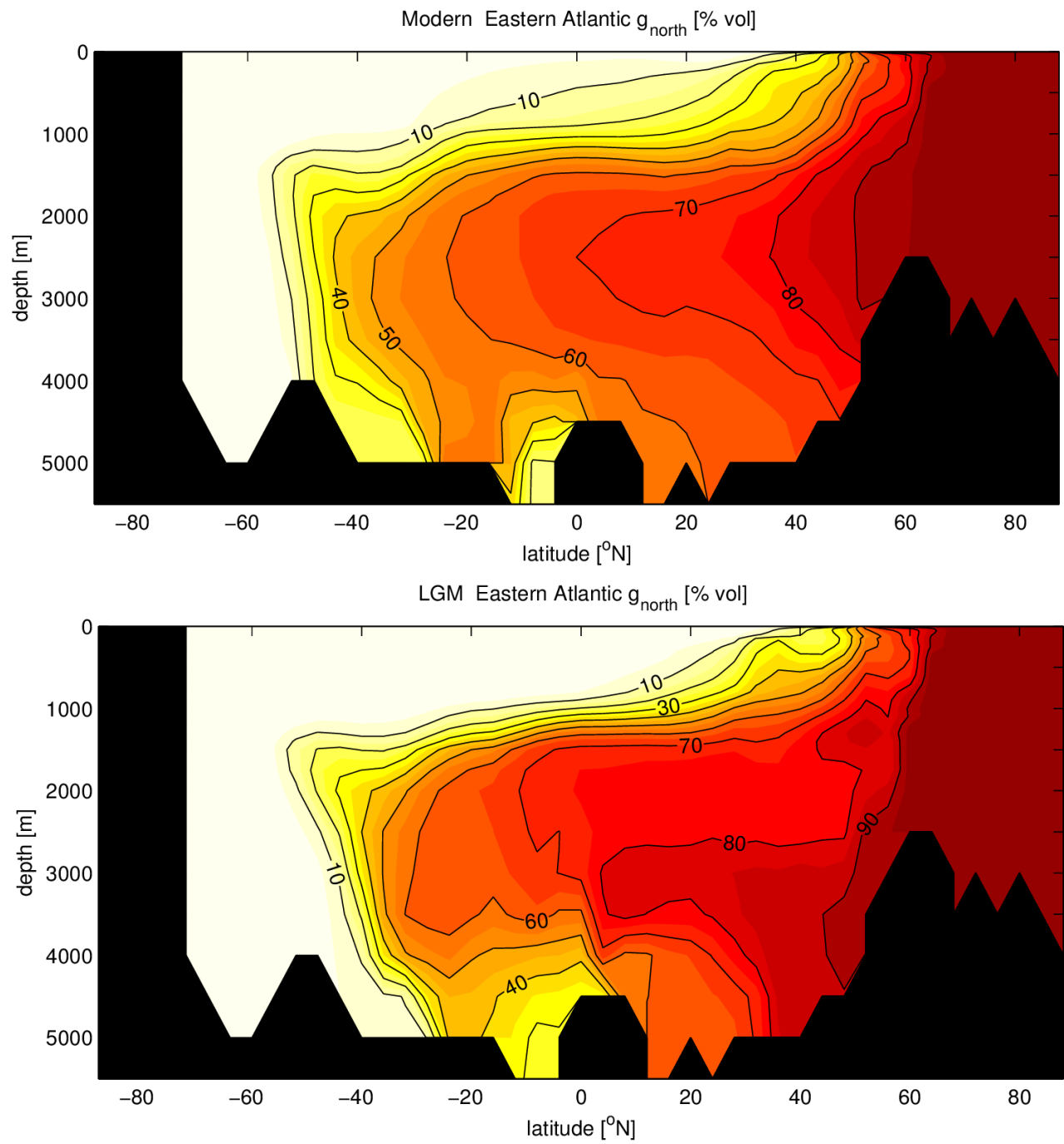**Figure 11.** Same as Figure 8, but for $\delta^{18}O_c$.

Figure 12. Same as Figure 8, but for North Atlantic Water concentration, $\mathbf{g}_{north}$.